Applied Surface Science 298 (2014) 137–141

Contents lists available at ScienceDirect

Applied Surface Science

journal homepage: www.elsevier.com/locate/apsusc

Formation of Au–Al alloy on silicon for polymer modulator electrode application

Yuanbin Yue, Jian Sun, Xuliang Zhao, Ying Xie, Xibin Wang, Lei Liang, Fei Wang, Changming Chen, Yunji Yi, Xiaoqiang Sun*, Daming Zhang

State Key Laboratory on Integrated Optoelectronics, Jilin University, Changchun, Jilin 130012, China

ARTICLE INFO

Article history:
Received 17 August 2013
Received in revised form 17 January 2014
Accepted 23 January 2014
Available online 2 February 2014

Keywords:
Anneal
AuAl
Alloy
Modulator

ABSTRACT

The formation of aurum–aluminum (Au–Al) alloy on silicon substrate and its use to be electrode of polymer electro-optic (EO) modulator were investigated. The surface morphology and crystallinity were studied by atomic force microscopy, scanning electron microscope, X-ray diffractometer (XRD) and energy dispersive spectrometer. The electrical resistivity was characterized by the four-probe method. XRD pattern confirmed the formation of AuAl phase. After annealed for 11 min at 575 °C, the Au–Al alloy film exhibited a root mean square roughness of less than 40 nm and a minimum electrical resistivity of 2.24 μΩ cm with no obvious change within 6 months. The scattering-parameter (S21) of a fabricated co-planar waveguide electrode polymer EO modulator was measured by vector network analyzer, and a 3-dB bandwidth of 5.2 GHz was observed. These physical properties promise good potentials of Au–Al alloy to be electrode of polymer EO modulators.

© 2014 Elsevier B.V. All rights reserved.

1. Introduction

Electro-optic (EO) modulators play key roles in a wide range of applications such as fiber-optic communications, phase-arrayed radar feeds, and analog/digital microwave links [1–3]. Many efforts have been devoted to improve the performance of EO modulators. The physical property of electrode is of great importance among factors that determine the fabrication and performance of modulators [4,5]. Commonly, aurum (Au) is adopted as the poling and ground electrode in polymer EO modulators. However, single Au layer on silicon substrate is easy to crinkle and lift off after spin-coating and cure of polymer cladding. This is owing to the thermal expansion coefficient difference of Au and polymers. An alternative approach is to use adhesion materials, such as titanium or chromium. However, these materials will diffuse into gold or gold alloy when an annealing temperature of about 400 °C is applied. No adhesion layer will be left and the adhesive function disappears.

The formation of aurum–aluminum (Au–Al) alloy on silicon has been investigated in bulk form for wafer bonding [6] which is applied in integrated circuits packaging or microelectromechanical systems [7,8], yet few studies have been conducted on gold aluminides in thin films geometry and their potential to be used as the poling and ground electrode of polymer EO modulators. As has been reported, the electrode surface morphology and resistance property are crucial for the performance of modulators because the protuberance on electrode may result in dielectric breakdown during electric poling, and high electrical resistivity will induce impedance mismatch and excess microwave transmission loss at high frequency [9,10]. Thus, the question concerning the mechanism of annealing temperature and time influence on characteristics of surface roughness and resistance of Au–Al alloy is still open to discuss.

In this work, a detailed study of Au–Al thin films is carried out. The physical property is presented as a function of temperature and time to optimize synthesizing parameters. The atomic force microscope (AFM) and four-probe electric measurement show that the Au–Al alloy exhibits a root mean square (RMS) roughness of less than 40 nm and an electrical resistivity of 2.24 μΩ cm when annealed for 11 min at 575 °C. X-ray diffractometer (XRD) pattern confirms the major phase of AuAl after annealing. Clear interfaces between layers and good adhesion of polymers on alloy electrode can be observed in scanning electron microscope (SEM) image. A 3-dB bandwidth of 5.2 GHz is measured from the fabricated polymer EO modulator with co-planar waveguide (CPW) upper electrode and Au–Al alloy ground electrode [11,12].

2. Experiments

The thermal evaporation method was used to deposit high-purity (>99.999%) solid Al and Au thin metal film with a thickness of 160 and 40 nm onto the p-type silicon wafer (1 0 0), sequentially

* Corresponding author. Tel.: +86 0431 851 680 97; fax: +86 0431 851 680 97.
E-mail address: sunxq@jlu.edu.cn (X. Sun).

0169-4332/$ – see front matter © 2014 Elsevier B.V. All rights reserved.
http://dx.doi.org/10.1016/j.apsusc.2014.01.141

www.spm.com.cn

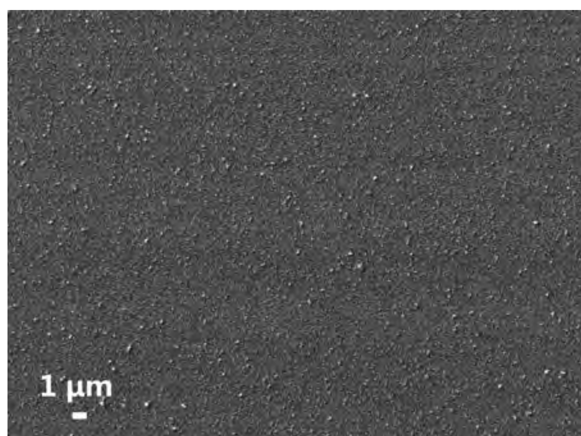

Fig. 1. SEM image of the Au–Al films surface morphology before annealing.

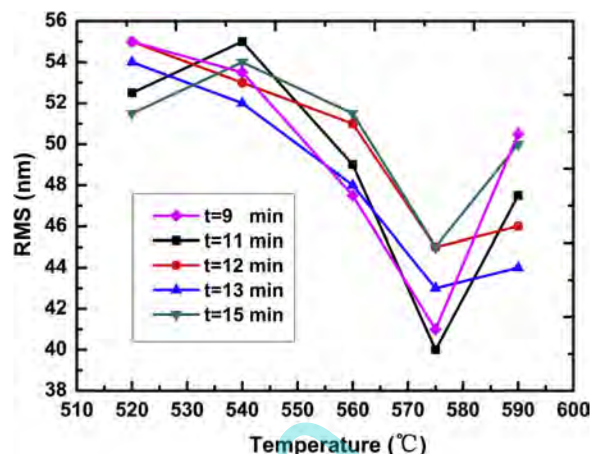

Fig. 2. RMS roughness as a function of annealing temperature and time.

[13,14]. The silicon wafer with metal films was then annealed in a home-made quartz oven with different temperatures and time in nitrogen ambient to avoid contamination and oxidation. The process began with a 5 min preheating at a lower temperature of 100 °C to release inner stress, then increasing at a heating rate of 80 °C/min. After several minutes annealing, post heating was adopted for 240 s, then cooled at a rate of 100 °C/min. The detailed morphology of sample was examined by means of SEM machine JSM-7600F (JEOL Ltd., Japan) that operated on voltage of 10 kV. AFM images were recorded with a multimode scanning probe microscope CSPM5000 (Being Nano-Instrument Ltd., China) that operated in contact mode to measure the RMS roughness on a 10 μm × 10 μm area. The crystal structure of the synthesized alloy was studied by a 6000 lab XRD machine (SHIMADZU Co., Japan). The electrical resistivity was measured by a SZT-2A four point probe tester (Tong-Chuang Co., China). A polymer EO modulator with CPW upper electrode and alloy ground electrode was fabricated according to the process in Ref. [15] to determine the 3-dB bandwidth. Norland Optical Adhesive 73 (NOA73) and Dispersed Red 1 (DR1) doped ultraviolet curable polymer SU-8 were adopted as the passive cladding and EO core layer, respectively. Before modulator performance measurement, it was sliced by a wafer dicing machine DAD-3220 (DISCO Co., Inc., Japan). Scattering-parameter (S21) was measured by a vector network analyzer 37269C (Anritsu Ltd., USA).

3. Results and discussion

To confirm the original state of metal film on silicon substrate, the pristine Au–Al film surface morphology is characterized by SEM image, as shown in Fig. 1. It can be seen that the surface is virtually featureless except for some particles, which is due to the tress effect induced by the interface energy difference between Al and Au.

When heated at low temperatures, an interdiffusion process will happen between Au and Al. This leads to a layers formation consisting of several intermetallics with different compositions, from Au-rich to Al-rich, with different growth rates. Cavities emerge when the denser and faster-growing layers consume slower-growing ones. This process leads to electrical resistance increasing, mechanical weakening and surface roughening. According to phase diagrams reported by Li et al. [16] and Liu et al. [17], Au–Al alloy will form at 520, 540, 560, 575 and 590 °C. Thus, they are chosen when investigating the RMS roughness of metal film surface as a function of annealing temperature and time, as shown in Fig. 2. The metal film presents a lowest RMS roughness of 40 nm at 575 °C when the processing time increases from 9 to 15 min. As the temperature is over 540 °C, the roughness shows the same evolution trends at all annealing time. However, different annealing time leads to RMS roughness changing reversely when the temperature increases from 520 to 540 °C. In fact, the absence of coexistence of Au and Al at the surface region implies the lack of Al–Au alloys, which is considered to be the major root cause of surface roughening [18].

In order to reveal the temperature effects on crystallization and profile, SEM investigation at different temperatures is performed when the annealing time is fixed at 11 min according to the above morphological analysis. Metal film cooling is accompanied with the formation of stable crystal phases, as well as metastable alloy in the zone of alloy formation. In Fig. 3(d), the growing process of intermetallic layers causes reduction in volume, and hence creates cavities in metal near the interface between Au and Al [19–21]. Meanwhile, the interface energy plays a key role in determining the final shape of Au–Al film after annealing. It may induce delamination between these two materials because aggregation of Au can minimize the interface energy through reducing contact area. Moreover, Piao and other co-workers [22–25] have shown how oxidation can occur in Au–Al thin films and affect surface morphology. At annealing temperature of 540 °C, Al exhibits coarse dendrites and grain shape, as shown in Fig. 3(a). With the annealing temperature increasing to 560 °C, strip microstructure of Al still exists, however the grain size becomes smaller to a certain extent, which reduces the surface roughness, as shown in Fig. 3(b) [26]. A compact and flat alloy film is observed in Fig. 3(c), which is in accordance with the interpretation in Refs. [16,27] that stable AlAu will formed at 575 °C. From study of the change in morphological and structural characteristics during heating Au–Al films on silicon, we discover that substantial differences from the bulk system exist in the formation of Au–Al alloy, except for some common features.

To reliably consider annealing treatments, the XRD pattern of sample annealed at 575 °C for 11 min is performed. Diffraction peaks located at about $2\theta = 30^\circ$ and 42° can be observed. A comparison with the standard diffractogram confirms the position of main peaks of AuAl, as shown in Fig. 4. As confirmed by XRD, AlAu is the major phase after annealing. Moreover, compared with the binary phase diagram of Au–Al system, the experimental agrees well with the phase diagram, which means significant diffusion of Au toward the metal/semiconductor interface has occurred after annealing. Specially, it is the reduction of Al_2Au and $AlAu_4$ that results in a smooth surface morphology [18].

As is well known, thin films show different resistivity behavior from the bulk material. It has been reported that thin copper or gold film shows a strong increase in electrical resistivity when its thickness decreases [17]. Thus, a resistance test through the four-probe method has been carried out. Fig. 5 shows the electrical resistivity as a function of annealing temperature. The resistivity mainly

www.spm.com.cn

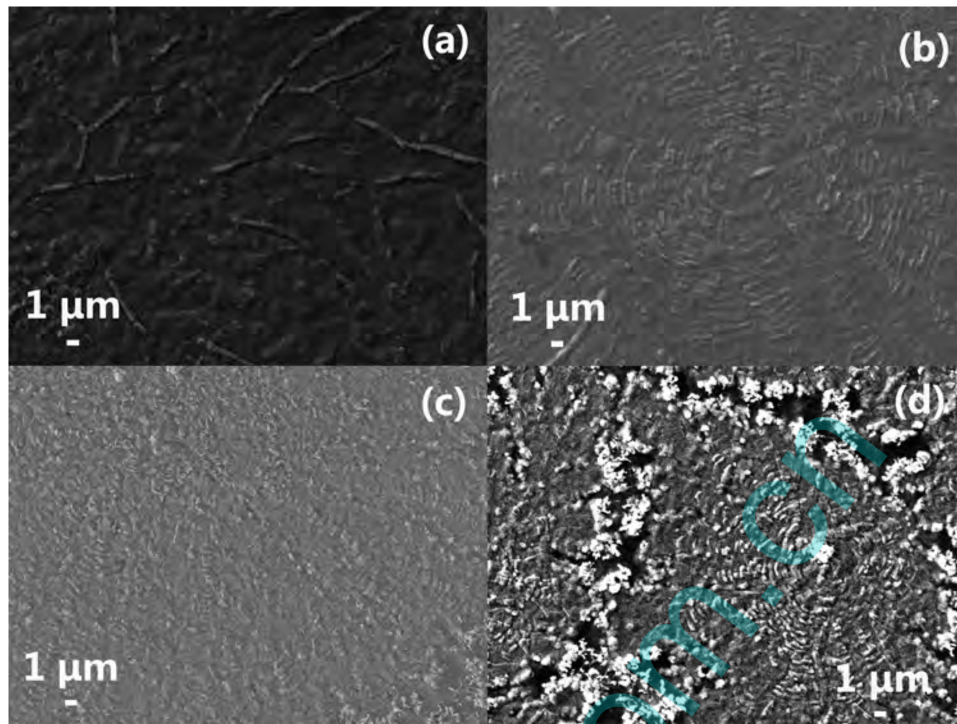

Fig. 3. SEM images of the Au–Al films morphology on silicon substrate when annealed at a temperature: (a) 540 °C, (b) 560 °C, (c) 575 °C, and (d) 590 °C.

maintains constant and is similar to the reported in Ref. [28]. A minimum value of 2.24 μΩ cm is found at the annealing temperature of 575 °C, keeping at a low level for a fixed film thickness. However, it is still a litter higher than the expected, which may be induced by the atmospheric air-oxygen or water existing into the oven. The pure ambient is hard to control, leading to an oxidation atmosphere during annealing process and resulting in higher resistivity. Furthermore, the time stability of AuAl is characterized to be increasing less than 1.3% after 3 months and 3.1% after 6 months, which is favorable to restrain resistance induced transmission loss and stabilize the modulator bandwidth, as shown in Fig. 5.

To confirm the existence of oxygen during annealing, element analysis is performed by means of energy dispersive spectrometer (EDS). As shown in Fig. 6, a weak oxygen signal is observed. Since Al and Au films are thermally evaporated on the silicon substrate in vacuum ambient sequentially, the existence of oxygen originates from the minimal amount of water existing in the oven, which may result in oxidation of aluminum during annealing though the process is carried out in nitrogen ambient [25]. However, this reaction on thin film surface is different from the oxidation of bulk Au–Al intermetallics that would otherwise affect the physical characteristics of alloy apparently [29]. As a result, the aluminide has not been detected by XRD because of its low content on film surface. Moreover, the above resistance test and the following frequency response test prove that oxidation no has no evident influence on electrical characteristics of alloy electrode. Hence, the Au–Al alloy can fulfill the electrical demand of modulator electrode.

Before modulator performance measurement, detailed interface investigation of polymer films is done. The interface morphology and cross section view of the inversed ridge waveguide are characterized by SEM machine, as shown in Fig. 7. A clear interface can be seen between DR1/SU-8 core layer and NOA73 claddings, which implies that no solvent erosion or dissolution has happened at the interface. This ensures optical nonlinearity stability of chromophores in the host polymer of SU-8. As shown in the inset of Fig. 7, no obvious roughness can be seen on the AuAl alloy surface,

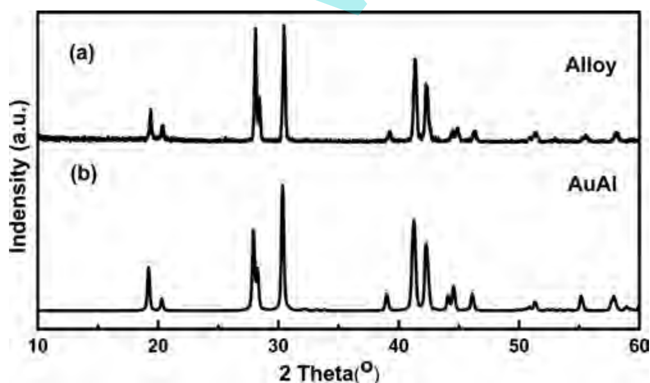

Fig. 4. XRD pattern of Au–Al films annealed at 575 °C for 11 min.

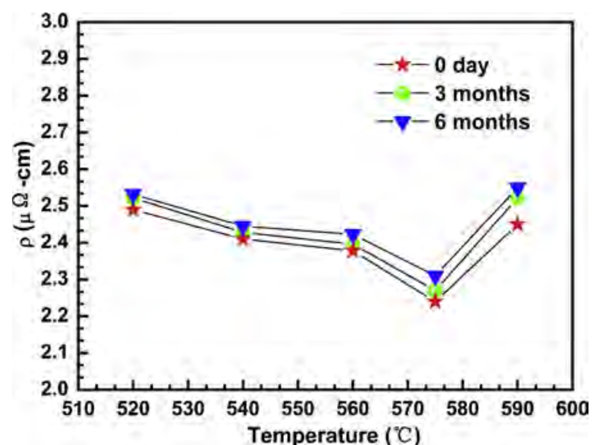

Fig. 5. Measured electrical resistivity of Au–Al films as a function of annealing temperature.

www.spm.com.cn

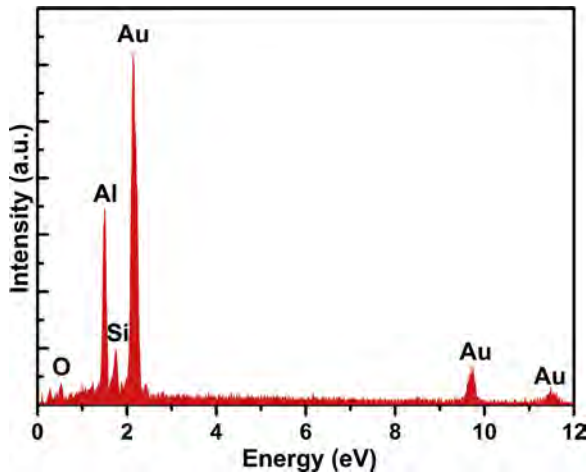

Fig. 6. EDS pattern of Au–Al films annealed at 575 °C for 11 min.

which is in accordance with the above AFM characterization. This smooth surface is favorable to reduce radiation loss and widen modulation bandwidth. Moreover, the good adhesion of polymer films on alloy surface can facilitate device fabrication and guarantee long time working stability.

For polymer EO modulators, optical nonlinearity is established by the application of a high poling electric field across the active layer of polymer stacks when heated to its glass transition temperature to preferentially align the chromophores, and then cooled down to room temperature to lock in the order. In this process, the electric field is chosen to be a critical value of just less than that would otherwise result in dielectric breakdown of polymers. As shown in Fig. 8, the breakdown voltage of film stacks and RMS of NOA73 cladding surface after poling are illustrated as a function of alloy electrode surface roughness that has been discussed in Fig. 2. Except for alloy surface roughness of 47.5 nm formed at the annealing temperature of 590 °C, both cladding surface roughness and breakdown voltage decrease with the increment of alloy surface roughness, which means that small surface roughness can reduce the probability of dielectric breakdown during high temperature poling. Consequently, the poling electric field inside the EO layer with smoother alloy electrode is higher than that with rougher electrode. This is favorable to establish stronger optical nonlinearity in EO layer. The fast falling of breakdown voltage at RMS of 47.5 nm is owing to the cavities and protuberances on alloy surface that

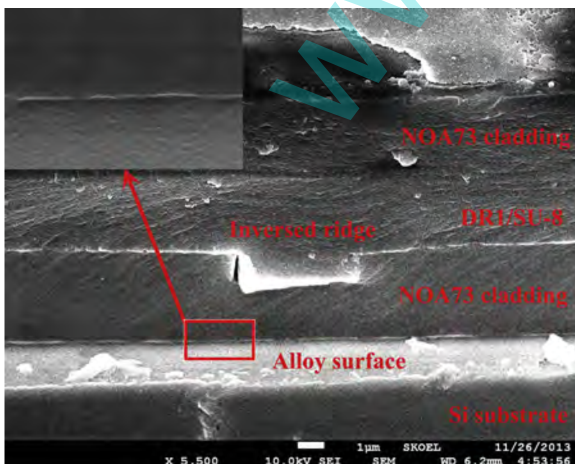

Fig. 7. SEM image of the cross-sectional view of EO modulator with Au–Al alloy electrode.

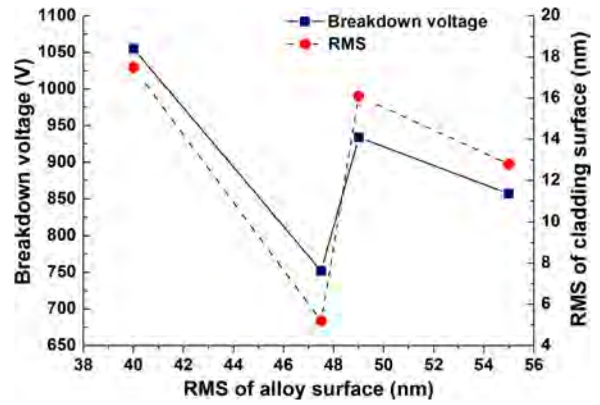

Fig. 8. RMS of cladding surface after poling and breakdown voltage of polymer stacks as a function of alloy surface roughness.

are likely to induce discharging across polymer stacks. Then this unsuccessful poling leads to a smoother cladding surface [30]. Furthermore, the amplification of EO polymer inhomogeneities during poling is an origin of optical loss for EO polymers and devices [30,31], smooth alloy can also prevent the poling induced refractive index decrement of the core and the subsequent loss of optical mode confinement [32].

According to the above characterization, the feasibility of Au–Al alloy as modulator electrode is confirmed by investigating S21 parameter of a Mach–Zehnder interferometer (MZI) modulator with CPW electrode. The magnitude of S21 in dB plotted against frequency over the range from 0 Hz to 6 GHz is shown in Fig. 9. Comparing with the reported work of a modulator with 3-dB bandwidth of 3.5 GHz, a relatively high 3-dB bandwidth of about 5.2 GHz is observed in Fig. 9, in view of the low thickness of upper Au electrode of 200 nm [33]. This bandwidth is mainly from the low phase mismatch between lightwave and microwave in polymer waveguide. Lower transmission loss and bandwidth improvement will be achieved if electroplating is used to optimize the thickness of upper Au electrode [4,34].

Moreover, the application of ground alloy electrode is favorable to optimize modulation depth and reduce half-wave voltage V_π. For a traditional MZI polymer EO modulator with micro-strip line (MSL) electrode, V_π can be expressed as

$$V_\pi = \frac{\lambda}{n_0^3 \gamma_{33}} \frac{G}{\Gamma L} \quad (1)$$

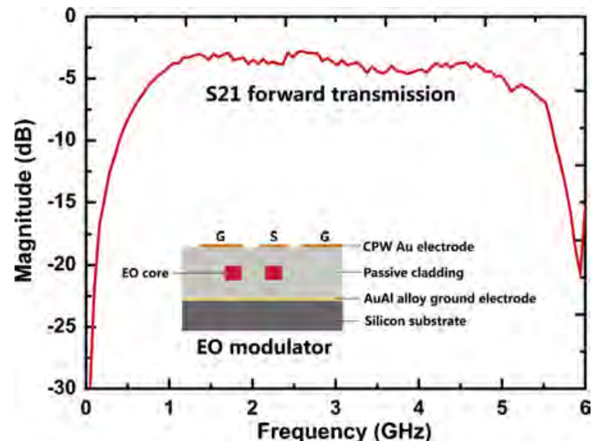

Fig. 9. Frequency response of a 3-dB bandwidth of 5.2 GHz with an inset image of the cross-sectional view of polymer EO modulator with CPW upper electrode and alloy ground electrode.

www.spm.com.cn

λ is the communication wavelength, n_0 is the refractive index of the EO material. It can be seen that V_π is mainly determined by modulation length L, gap between voltage electrodes G, EO coefficient γ_{33}, and EO overlap integration factor Γ that corresponds to the signal electric field distribution in optical waveguide layers normalized to the field that would be there if air were the dielectric [35,36], expressed by Eq. (2)

$$\Gamma = \frac{\iint_{oe} E_e(x, y) \cdot |E_o(x, y)|^2 \, dxdy}{\int_{-\infty}^{\infty} \int_{-\infty}^{\infty} |E_o(x, y)|^2 \, dxdy} \tag{2}$$

According to Eq. (1), for fixed material characteristics and waveguide configuration, Γ should be increased to lower V_π. To study the effects of electrode performance to Γ, the electric field distributions in the waveguide with and without Au–Al alloy ground electrode have been calculated, respectively. The results show that Γ increases from 47.43% to 89.52%, which confirms the validity of adopting alloy electrode to improve the performance of polymer EO modulators [37].

4. Conclusions

Bilayers of Au–Al are deposited on silicon substrate to form alloy by annealing process and used as the electrode of modulators. Our investigation of morphological and structural characteristics during annealing shows that the temperature and time have substantial impacts on the surface roughness and compositions of alloy. Corresponding AuAl diffraction peaks are observed in the XRD pattern. The alloy exhibits favorable performances of a RMS roughness of 40 nm and an electrical resistivity of 2.24 μΩ cm when annealed at 575 °C for 11 min. These favorable characteristics can improve poling electric field in waveguide effectively. The measured S21 parameter of the MZI modulator shows a 3-dB bandwidth of 5.2 GHz. Our investigation proves that Au–Al alloy can fully meet the requirement of being poling and ground electrode of polymer EO modulators.

Acknowledgements

This work is supported by the National Natural Science Foundation of China (nos. 61177027, 61107019, and 61205032), Program for Special Funds of Basic Science & Technology of Jilin University (nos. 201100253 and 201103071), and China Postdoctoral Science Foundation (no. 2012M510900).

References

[1] Y. Enami, C.T. DeRose, C. Loychik, D. Mathine, R.A. Norwood, Applied Physics Letters 89 (2006) 143506.
[2] J. Han, B.-J. Seo, S.K. Kim, H. Zhang, H.R. Fetterman, IEEE Journal of Lightwave Technology 21 (2003) 3257.
[3] L. Dalton, A. Harper, A. Ren, F. Wang, G. Todorova, J. Chen, C. Zhang, M. Lee, Industrial and Engineering Chemistry Research 38 (1999) 8.
[4] M. El-Gibari, D. Averty, C. Lupi, H. Li, S. Toutain, Microwave and Optical Technology Letters 52 (2010) 1078.
[5] C. Zheng, L. Zhang, L.C. Qv, L. Liang, C.S. Ma, D. Zhang, Z. Cui, Optical and Quantum Electronics 45 (2013) 279.
[6] A.L. Pinardi, S.J. Leake, R. Felici, I.K. Robinson, Physical Review B 79 (2009) 045416.
[7] P.H. Chen, C.L. Lin, C.Y. Liu, Applied Physics Letters 90 (2007) 132120.
[8] L. Tang, F. Li, Q. Guo, Applied Surface Science 258 (2011) 1109.
[9] K. Liang, Q. Song, F. Lu, B. Wu, W. Chen, H. Peng, C. Liu, S. Luo, Fiber and Integrated Optics 24 (2005) 521.
[10] C. Algani, N.E. Belhadj-Tahar, F. Deshours, J.L. Montmagnon, P. Roduit, G. Alquié, C. Fortin, 35th European Microwave Conference, Paris, France, October 4–6, 2005, p. 1287.
[11] H. Huang, S.R. Nuccio, Y. Yue, Journal of Lightwave Technology 30 (2012) 3647.
[12] D.J. Thomson, F.Y. Gardes, J.-M. Fedeli, IEEE Photonics Technology Letters 24 (2012) 234.
[13] Q. Wan, T.H. Wang, C.L. Lin, Applied Surface Science 221 (2004) 38.
[14] S. Takeda, H. Fujii, Y. Kawakita, S. Tahara, S. Nakashima, S. Kohara, M. Itou, Journal of Alloys and Compounds 452 (2008) 149.
[15] C.M. Chen, F. Zhang, H. Wang, X.Q. Sun, F. Wang, Z.C. Cui, D.M. Zhang, IEEE Journal of Quantum Electronics 47 (2011) 959.
[16] M. Li, C. Li, F. Wang, D. Luo, W. Zhang, Journal of Alloys and Compounds 385 (2004) 199.
[17] H.S. Liu, J. Wang, Y. Du, Z.P. Jin, Zeitschrift fur Metallkunde 95 (2004) 45.
[18] Z. Bao, A. Dodabalapur, A.J. Lovinger, Applied Physics Letters 69 (1996) 4108.
[19] B.P. Luther, S.E. Mohney, T.N. Jackson, M.A. Khan, Q. Chen, J.W. Yang, Applied Physics Letters 70 (1997) 57.
[20] M.E. Lin, Z. Ma, F.Y. Huang, Z.F. Fan, L.H. Allen, H. Morkoc, Applied Physics Letters 64 (1994) 1003.
[21] S.N. Mohammad, Journal of Applied Physics 95 (2004) 7940.
[22] H. Piao, M. Suominen Fuller, D. Miller, N.S. McIntyre, Applied Surface Science 187 (2002) 266.
[23] H. Piao, N.S. McIntyre, Surface Science 421 (1999) 171.
[24] H. Piao, N.S. McIntyre, Surface Interface Analysis 31 (2001) 874.
[25] H. Piao, N.S. McIntyre, Journal of Electron Spectroscopy Related Phenomena 119 (2001) 29.
[26] Q. Wang, Z. Zhang, F. Long, B. Guo, H. Geng, Transactions of the Indian Institute of Metals 66 (2013) 257.
[27] J.M. Camacho, OlivaF A.I., Microelectronics Journal 36 (2005) 555.
[28] W. Zhang, S.H. Brongersma, O. Richard, B. Brijs, R. Palmans, L. Froyen, K. Maex, Journal of Vacuum Science and Technology B 22 (2004) 2715.
[29] C. Xu, C.D. Breach, T. Sritharan, F. Wulff, S.G. Mhaisalkar, Thin Solid Films 462 (2004) 357.
[30] X. Sun, Y. Xie, X. Zhao, S. Zhao, D. Li, X. Wang, J. Sun, L. Liang, C. Chen, D. Zhang, F. Wang, Z. Xie, Applied Surface Science 285 (2013) 469.
[31] C.C. Teng, M.A. Mortazavi, G.K. Boudoughian, Applied Physics Letters 66 (1995) 667.
[32] H. Zhang, M.C. Oh, A. Szep, W.H. Steier, C. Zhang, L.R. Dalton, H. Erlig, Y. Chang, D.H. Chang, H.R. Fetterman, Applied Physics Letters 78 (2001) 3136.
[33] W. Gao, J. Sun, X. Sun, Y. Yan, L. Gao, D. Zhang, Microwave and Optical Technology Letters 51 (2009) 2097.
[34] S.K. Kim, K. Geary, H.R. Fetterman, C. Zhang, C.W.H. Wang, W.H. Steier, Electronics Letters 39 (2003) 1321.
[35] Y. Shi, C. Zhang, H. Zhang, J.H. Bechtel, L.R. Dalton, B.H. Robinson, W.H. Steier, Science 288 (2000) 119.
[36] M. Lee, H.E. Katz, C. Erben, D.M. Gill, P. Gopalan, J.D. Heber, D.J. McGee, Science 298 (2002) 1401.
[37] J. Sun, C. Chen, L. Gao, X. Sun, W. Gao, C. Ma, D. Zhang, Optics Communications 282 (2009) 2255.

www.spm.com.cn